JOURNAL OF MATERIALS SCIENCE **34** (1999) 4385–4392

Dense Ti_3SiC_2 prepared by reactive HIP

N. F. GAO, Y. MIYAMOTO
Joining and Welding Research Institute, Osaka University, Ibaraki 567, Osaka, Japan
E-mail: nfgao@jwri.osaka-u.ac.jp

D. ZHANG
State Key Lab of Metal Matrix Composites, Shanghai Jiao Tong University, No. 1954 Huashan Rd., Shanghai 200030, People's Republic of China
E-mail: zhangdi@mail.sjtu.edu.cn

The dense polycrystalline Ti_3SiC_2 has been synthesized by reactive HIPing of Ti, SiC and C powders. The bulk material with the highest Ti_3SiC_2 content about 97 vol % was obtained when treated at 1500 °C, 40 MPa for 30 min. The density was 99% of the theoretical value. The Ti_3SiC_2 grains had the columnar and plate-like shapes. The grains were well boned to form a network structure. Many stacking faults were observed along the (001) plane of Ti_3SiC_2. The Vickers hardness, Young's modulus, flexural strength and fracture toughness were 4 GPa, 283 GPa, 410 MPa and 11.2 MPa $m^{1/2}$, respectively. The Ti_3SiC_2 was stable up to 1100 °C in air. The electrical resistivity was 2.7×10^{-7} Ω·m at room temperature. The resistivity increased linearly with the increasing temperature. It may be attributed to a second order phase transition. The Seebeck coefficient was from 4 to 20 μV/K in the temperature range 300–1200 K. It seems that Ti_3SiC_2 is semi-metallic with hole carriers from this small positive value.

1. Introduction

Ti_3SiC_2 is known as a ductile ceramic with high Young's modulus and low hardness. The first successful synthesis of Ti_3SiC_2 was carried out via chemical reaction of TiH_2, Si and graphite at 2000 °C by Jeitschko and Nowotny [1]. Goto and Hirai synthesized polycrystalline plates by CVD method using $SiCl_4$, $TiCl_4$, CCl_4 and H_2 as source gases [2]. Some investigations on welding of Ti and SiC showed that the formation of Ti_3SiC_2 compound resulted in high bonding strength [3]. However the gaseous reaction method like CVD is limited in a small-scale production. Various solid state synthesis methods via different starting materials were tried in order to fabricate bulk monolithic Ti_3SiC_2. Racault *et al.* fabricated nearly pure Ti_3SiC_2 by vacuum calcination of starting Ti/Si/C powders and subjected the products to chemical treatment so as to remove $TiSi_2$ and TiC impurities [4]. Arunajatesan and Carim reported that by arc melting of Ti/Si/C powders and annealing at 1200 °C for 100 h the monolithic material containing 98 vol % of Ti_3SiC_2 could be obtained [5]. Okano *et al.* tried to synthesize Ti_3SiC_2 by reactive sintering of Ti/Si/TiC in vacuum at the temperature range of 1300–1600 °C. They reported that the optimal processing temperature was 1300 °C. The products apparently contained small volume of TiC and SiC as secondary phases, which were further densified by hot pressing (1400 °C, 45 MPa, 30 min). The sintered body demonstrated a fracture toughness of 6.9 MPa $m^{1/2}$. The flexural strength was 560 MPa at room temperature and 500 MPa at 1000 °C [6].

Our previous work was focused on the combustion synthesis of Ti_3SiC_2 with Ti/Si/C powders. But the products contained TiC_x phase. After HIP sintering we made an extrapolation of the Vickers hardness with the content of TiC_x phase and proposed that the Vickers hardness of the pure polycrystalline Ti_3SiC_2 would be 4 GPa [7]. Other processing methods such as the pulse electric current sintering were being investigated by other researchers [8].

More recently, Barsoum and El-Raghy claimed that they could produce highly pure bulk crystalline Ti_3SiC_2 by hot pressing the Ti/SiC/C mixtures at 1600 °C for 4 h. However, judging from the published X-ray diffraction pattern the $TiSi_2$ secondary phase seems to remain in the products [9].

The Ti_3SiC_2 possesses attractive properties such as high electrical conductivity, high oxidation and chemical resistance, excellent high temperature strength, high thermal shock resistance and self-lubricating which may enable it to future applications such as commutating brushes for motors, armor, bearing, turbine blades and so on.

These unique characteristics of Ti_3SiC_2 arouse the interest to synthesize the dense and pure Ti_3SiC_2. But the fabrication of pure monolithic Ti_3SiC_2 is limited in a small scale of CVD or long time annealing method so far. Since intrinsic properties of Ti_3SiC_2 are still not clear, this study attempted to synthesize and densify the pure Ti_3SiC_2 by reactive HIP sintering of Ti/SiC/C powders. Subsequently the products were investigated to clarify the intrinsic properties of polycrystalline

TABLE I Characteristics of raw powders

Raw materials	Purity (%)	Size (μm)	Product name	Manufacturer
Ti	99.6	<45	TSPT-350	Osaka Titanium Co., Ltd.
SiC	98.7	0.3	Bettarundum	Nihon Kokuen Co., Ltd.
Graphite	96.3	0.5	SP 300	Ibiden Co., Ltd.

Ti_3SiC_2 such as sintering behaviour, microstructure, mechanical and electrical properties, and oxidation resistance.

2. Experimental

Commercially available Ti, β-SiC and graphite powders were used to synthesize and densify the Ti_3SiC_2 by reactive HIP sintering. The characteristics of starting powders are shown in Table I. The above powders were mixed according to a molar ratio of 3Ti : Si : 2C. After ball milling in ethanol for 24 h, the powders were vacuum dried and then CIPed into a green body at 200 MPa. The green body ($\phi 35 \times 10$ mm) was vacuum (0.01 Pa) sealed into a Pyrex glass capsule with BN powder bed [10]. Then the capsule was placed into a graphite die and HIP processed under various conditions. The temperature, pressure and time ranges were 1300–1600 °C, 40–100 MPa and 0.5–4 h, respectively.

The sintered products were characterized by XRD method to determine the phase composition and lattice parameters. The lattice parameters were measured with Si as a standard reference. The phase content was determined by means of standard additive method. Density of a sintered body was measured by Archimedes' method. The measured density was evaluated comparing with the theoretical density derived from lattice constants. The microstructure was observed by using OM, SEM and TEM.

Measurement of Vickers hardness was carried out at various loads from 9.8 to 98 N for 15 s. The surface of a sintered body was polished with diamond paste. The ultra- micro Vickers hardness data were collected by UMIS (Ultra-Micro Indentation System)-2000 system [11]. This system allows indentation with multiple partial unloading by spherical indenter or load cycle indentation by Vickers indenter. The nominal radius of diamond spherical indenter is 5 μm. It is effective to characterize mechanical properties for small volumes of material. By this method, the intrinsic mechanical properties of Ti_3SiC_2 were distinguished from the TiC_x phase included in the products. The Young's modulus was calculated from the composite modulus expression.

Flexural strength was measured with cross head speed of 0.5 mm/min by 3-point bending method. Fracture toughness measurement was conducted by SEPB method with the specimen dimensions of $3 \times 4 \times 18$ mm. The pre-crack was introduced by indentation in the middle of a specimen. Optical microscope was used to measure the average length of the pre-crack.

The friction characteristic of Ti_3SiC_2 as a function of temperature was evaluated by unlubricated reciprocal sliding between a block sample and an Al_2O_3 ball (ϕ10 mm) [12]. The contact load and sliding speed were 9.8 N and 60 cycle/min, respectively.

The oxidation behaviour was examined by means of TG and DTA. The oxidized phase was identified by EDX and XRD analyses. Four probe method was used to measure the change of electrical resistivity with temperature up to 850 °C. The Seebeck coefficient was evaluated up to 900 °C in vacuum.

3. Results and discussion

3.1. Phase identification

Fig. 1 shows X-ray diffraction patterns of sintered samples. Two different phases of Ti_3SiC_2 and TiC_x were identified. When reactive HIP processed at 1500 °C and 40 MPa for 30 min, the main peak intensity of TiC_x is the weakest compared with the peak intensity of Ti_3SiC_2. The lattice parameters of TiC_x and Ti_3SiC_2 were $a = 0.43200(2)$ nm and $a = b = 0.3069(1)$ $c = 1.7697(2)$ nm, respectively. It is reasonable to assume 0.75 for carbon ratio in TiC_x referring to the relation between x and lattice constant [13]. The theoretical densities of TiC_x and Ti_3SiC_2 were estimated to be 4.68 and 4.50 g/cm^3, respectively. Under all the processing conditions, the lattice parameters of Ti_3SiC_2 remained almost unchanged.

In order to calculate the volume content of Ti_3SiC_2, the pure TiC powder was mixed with the pulverized product in different weight ratios. Good linear fitness was made according to the ratio of (200) and (104) peak intensities of TiC_x to that of (104) peak in Ti_3SiC_2, respectively as shown in Fig. 2. The weight percentage of

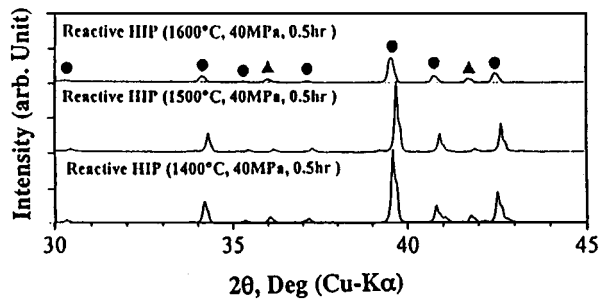

Figure 1 X-ray diffraction patterns of the sintered products, ●: Ti_3SiC_2, ▲: TiC_x.

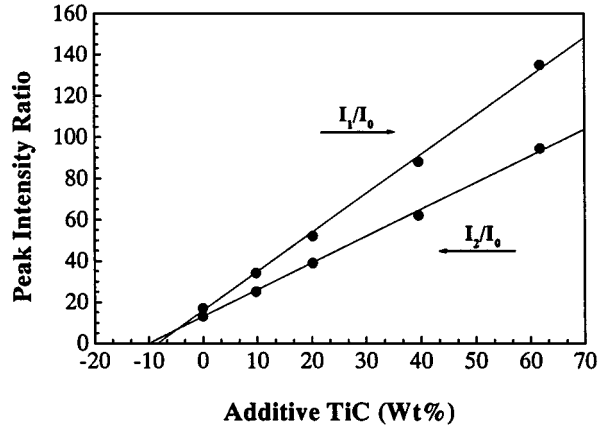

Figure 2 Calibration lines for X-ray standard additive method, I_0 is the peak intensity of (104) for Ti_3SiC_2, I_1 and I_2 is the peak intensity of (200) and (111), respectively.

TiC was an average of the two values from the extrapolation. The corresponding volume percentage of each phase was deduced from the above theoretical density values.

The most pure dense sample included 97 vol % of Ti_3SiC_2 which was prepared at 1500 °C and 40 MPa for 30 min by reactive HIP. The density was 4.46 g/cm^3 which is 99% of theoretical. The density, composition and Vickers hardness of the products prepared by various processing conditions are listed in Table II.

Fig. 3 shows the density and the phase content as a function of HIP temperature. When reactive HIP processed at 40 MPa for 30 min there was a temperature range at around 1500 °C that favored the formation of Ti_3SiC_2. When the temperature dropped from 1500 to 1300 °C the volume content of Ti_3SiC_2 decreased drastically from 97 to 55%. When applying the HIP process at 1600 °C for various time at various pressures the content of Ti_3SiC_2 didn't change substantially.

TABLE II Processing conditions and products' properties

Sample no.	Conditions T (°C)	P (MPa)	t (h)	ρ (g/cm^3)	H_v(GPa) (9.8 N)	Ti_3SiC_2 (vol %)
1	1300	100	1	4.32	13.5	55
2	1400	40	0.5	4.44	4.4	95
3	1500	40	0.5	4.46	3.9	97
4	1600	100	1	4.53	4.6	91
5	1600	40	0.5	4.53	4.5	92

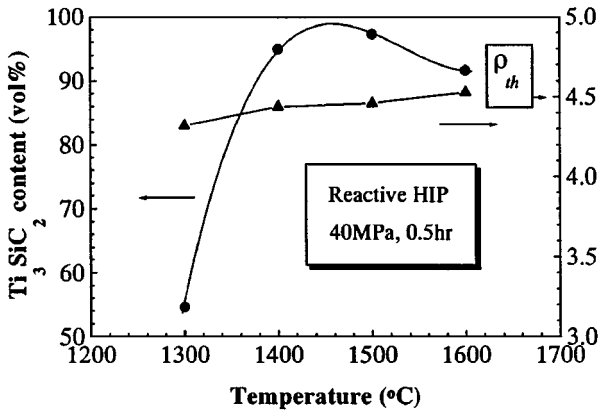

Figure 3 Density and phase content vs. HIP temperature.

3.2. Microstructure observation

Fig. 4 shows the etched surface of the sintered body. The columnar Ti_3SiC_2 grains with a bright center ridge and the plate-like grains with striated etched lines are readily distinguished. The bright small and acute blocks locating among Ti_3SiC_2 grains are TiC_x as seen in Fig. 4c. EDX analysis indicated that the Ti_3SiC_2 had a composition range to some extent. Some TiC_x grains contained Si up to 10 at %.

The processing temperature affected the grain size of Ti_3SiC_2 and TiC_x. When reactive HIP processed at 1400 °C and 40 MPa for 0.5 h, the average size of Ti_3SiC_2 was about 20 μm and TiC_x about 1 μm as seen in Fig. 4a. The small TiC_x phase was evenly distributed in Fig. 4b that was in agreement with the least volume fraction of TiC_x as determined by X-ray analysis when HIP sintered at 1500 °C and 40 MPa for 0.5 h. At 1600 °C and 100 MPa, the Ti_3SiC_2 content didn't changed as holding time increased from 0.5 to 4 h. Only TiC_x grains grew to about 10 μm, see Fig. 4d. The most pure and dense Ti_3SiC_2 was obtained at 1500 °C. As the HIP temperature was reduced to 1300 °C, both the formation and densification of Ti_3SiC_2 were suppressed.

The crystal structure of Ti_3SiC_2 consists of Ti_3C_2 octahedrons stacked in the C axis and separated by layers of Si atoms. The high elastic modulus and low hardness of Ti_3SiC_2 may be attributable to the combination of strong Ti-C bonds and weak bonds between Si layers and Ti_3C_2 octahedrons.

The high magnification TEM micrograph associating with SAED revealed that the stacking faults laid

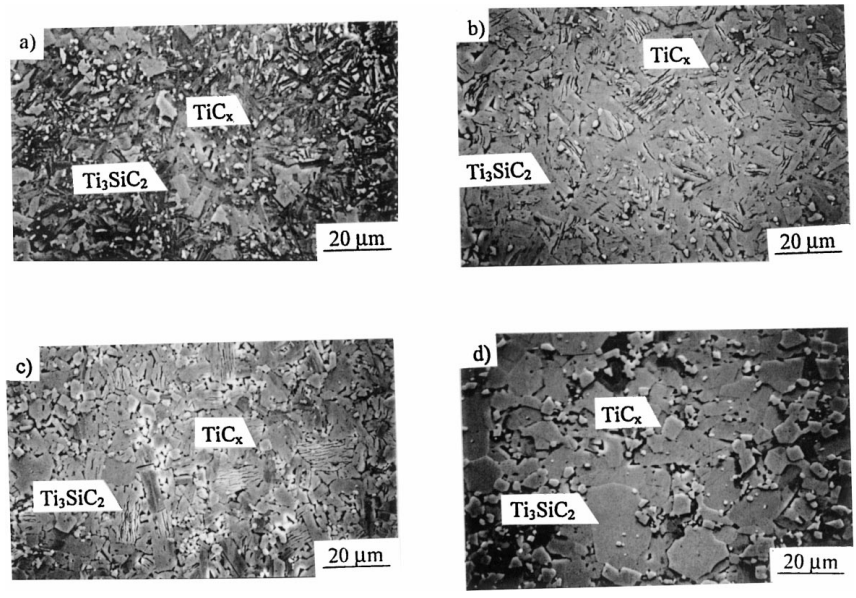

Figure 4 SEM micrographs of HIPed samples for (a) (1400 °C, 40 MPa, 0.5 h), (b) (1500 °C, 40 MPa, 0.5 h), (c) (1600 °C, 40 MPa, 0.5 h) and (d) (1600 °C, 40 MPa, 4 h).

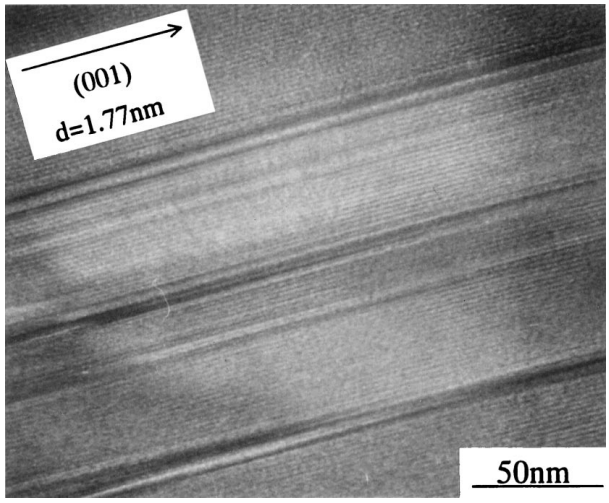

Figure 5 TEM micrograph of stacking faults on (001) plane.

on (001) plane of Ti_3SiC_2 (see Fig. 5). Considering the arrangement of columnar and plate-like images in SEM micrograph, the Ti_3SiC_2 grains seem to be thin flat plates. The *c*-axis is perpendicular to the plate. In hexagonal Ti_3SiC_2, the slip system is very limited. The c/a value is large and the bonding between Si layers and Ti_3C_2 octahedrons is weak. In these crystallographic constraints, the stress would be induced by the pressurization, cooling and intersecting grain growth during the process, and relaxed by forming stacking faults on (001) plane. These stacking faults are susceptible to stress and normally act as a source of cracks. Especially when the grain size is large, the stacking faults on the basal plane will lead to large cleavage fracture and strength degradation. However, this kind of anisotropic strength can cause deflection or arrest of crack propagation. Moreover, the tangling of columnar grains can improve the toughness and strength of Ti_3SiC_2.

Fig. 6 is a TEM micrograph at the triple junction of grains. The upper grain is Ti_3SiC_2 and the lower ones are TiC_x. The grain boundary and the triple point contained neither pore nor any reaction phase.

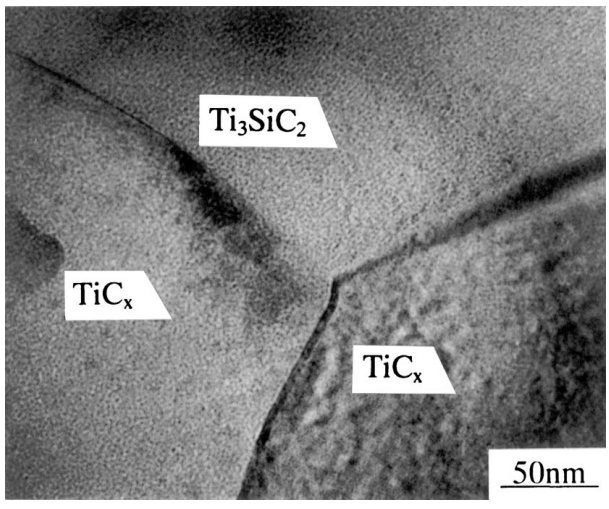

Figure 6 TEM micrograph of triple joints of Ti_3SiC_2 and TiC_x.

TABLE III Young's modulus and micro Vickers hardness by UMIS

		H_v(GPa)	
	E(GPa)	(49 mN)	(490 mN)
Ti_3SiC_2	283	12.7	9.7
TiC_x	361	17.0	14.7

3.3. Mechanical properties

3.3.1. Hardness and Young's modulus

The ultra-micro Vickers hardness and Young's modulus were measured by using the UMIS system. Fig. 7a and b show the Vickers indentation force as a function of applying load and the calculated mean pressure in load cycle. The mean pressure was converted to the hardness. Table III compares the hardness and Young's modulus measured on the Ti_3SiC_2 and TiC_x phase areas.

The stress-strain curve in Fig. 7d was obtained from the partial unloading curves (Fig. 7c) of ultra-micro spherical indentation. In the elastic-plastic model of spherical indentation the principal representative stress and strain are expressed as $P_m = P/\pi a^2$ and $\varepsilon_r = 0.2a/R$, respectively, where a is the radius of indentation, R the radius of indenter and P the indentation load. The expression is valid when the indentation depth is less than $3/R$ [11]. It can be seen that 0.3 is the critical value from the elastic to plastic deformation during indentation. The Young's modulus was calculated to be 283 GPa. Pampuch *et al.* reported 326 GPa [14]. Considering that their samples contained 10–30% TiC_x with higher modulus, it is reasonable to take 283 GPa as the intrinsic Young's modulus for Ti_3SiC_2. The strain-hardening index of Ti_3SiC_2 was estimated to be 0.484, which is near the value of 18-8 stainless steel.

Fig. 8 shows the load dependence of Vickers hardness for the samples prepared at 1500 °C, 40 MPa and 0.5 h. When the load was as low as 49 mN, the Vickers hardness was 12.7 GPa, it decreased with the increasing load and stopped at about 4 GPa for 9.8 N load. Goto and Hirai reported that the CVD derived Ti_3SiC_2 showed the constant Vickers hardness of about 6 GPa in the 0.98–9.8 N load range and the scattered hardness was attributed to the anisotropy of microstructure [2]. The high Vickers hardness at low indentation loads measured in the present study is probably due to the elastic recovery that produces a smaller indentation size after indentation. Therefore, the value of 4 GPa can be regarded as the intrinsic hardness of polycrystalline Ti_3SiC_2. It is in accordance with the predicted value for the polycrystalline material by the extrapolation method [7] and the measured value by Barsoum and El-Raghy [9].

The morphology of Vickers indentation was entirely different depending on the content of Ti_3SiC_2. Micrographs in Fig. 9 compares the indentation of samples. Fig 9a shows the indentation of sample 3 of high purity. The bright matrix is Ti_3SiC_2 and only a small volume of gray TiC_x phase exists in the view. The indentation was quite irregular with the peeled off bits and deformed material. Median or lateral cracks were invisible suggesting the ductile nature of Ti_3SiC_2. The damage

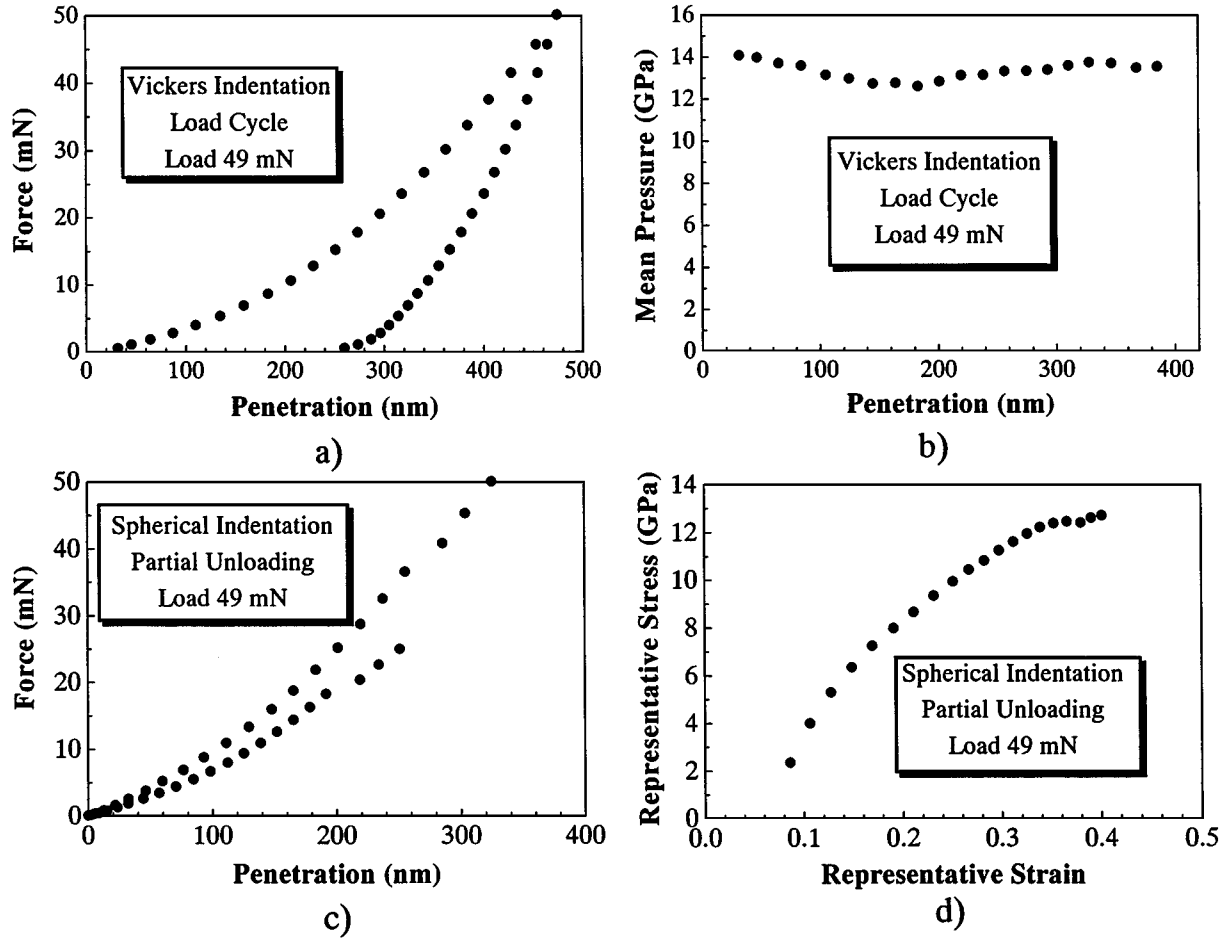

Figure 7 Results of ultra-micro indentation experiments on Ti_3SiC_2, (a) cycle load vs. indenter penetration, (b) the corresponding mean pressure vs. plastic penetration, (c) partial unloading load vs. indenter penetration, (d) the corresponding representative stress vs. strain.

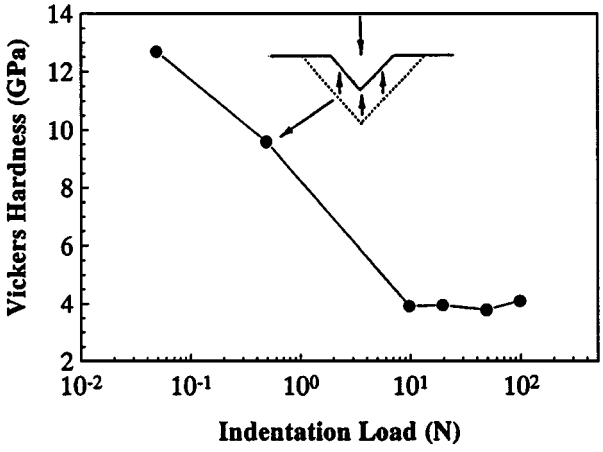

Figure 8 Load dependence of Vickers hardness.

around the indentation was unsymmetrical. The damage area extended to about 50% of the indentation size. No detectable cracks were produced. Some of the material around the indentation exfoliated during unloading. From some parallel slip lines we can infer the orientation of grains. Fig. 9b is a side view of indentation of sample 3. The sink in and pile up of the material around the indentation was clearly observed, that normally occurs in metal. This phenomenon indicated the plasticity of Ti_3SiC_2. Fig. 9c shows an indentation on a large TiC_x grain. It clearly demonstrated the brittle nature of ceramics. The lateral cracks propagated in TiC_x for a distance but stopped in the tough Ti_3SiC_2 area. In the periphery of Ti_3SiC_2, some slip lines produced for the load transfer.

From the above observation we can suppose that the indentation deforming behaviour of Ti_3SiC_2 is mainly due to slipping and debonding at the weak bonds between the Ti_3C_2 octahedrons and Si layers. This assumption seems to be supported by SEM and TEM observations as well. In Fig. 9a, the indentation size is around 70 μm, and the grain size is about 10–20 μm. The grains on the right wall of indentation are in the favorable orientations for deformation under stress induced by indentation. When the basal plane of a grain is parallel to the shear stress the deformation by slipping and debonding should occur. The grains on the left wall might not fit to the deformation orientation and crushed to crisp exfoliation. With other mechanism like intersection of columnar grains, crack deflection at the basal plane and detention of crack propagation the Ti_3SiC_2 demonstrates the ability to suppress the deformation damage in the local area.

3.3.2. Fracture toughness and flexural strength

The reactive HIP processed Ti_3SiC_2 (1600 °C, 40 MPa, 0.5 h) demonstrated the fracture toughness of 11.2 ± 0.5 MPa $m^{1/2}$. It is about 60% higher than the reported value by Okano *et al.* [6]. The transgranular fracture

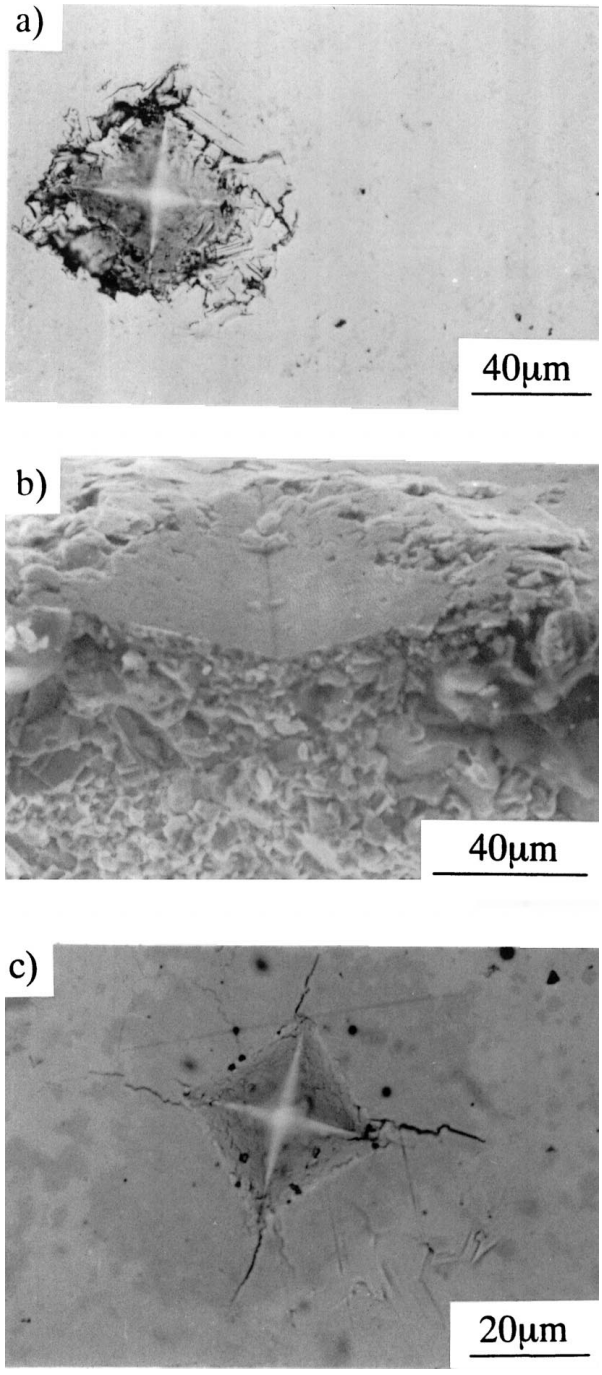

Figure 9 Comparison of Vickers indentation (a) indentation on sample 3, (b) the corresponding side view of the indentation, and (c) indentation on TiC_x phase.

was observed as shown in Fig. 10. The fracture surface is quite rough with many steps along the cleavage faces. The cleavage surface corresponds to the crystallographic basal plane. The columnar and platelet shape grains with layer structure would contribute to the high fracture toughness of Ti_3SiC_2. The flexural strength of the reactive HIP sample was 410 ± 25 MPa. This value is 58% higher than that of the hot processed Ti_3SiC_2 [9]. Some large cleavage surfaces about 30–50 μm in size were observed. Higher strength may be obtained by controlling the grain size of Ti_3SiC_2.

3.3.3. Friction characteristic

Fig. 11 shows the friction coefficient of sample 5 as a function of temperature. At room temperature the

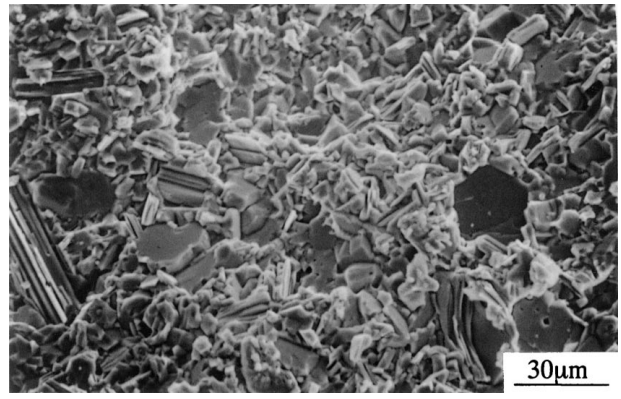

Figure 10 Fracture surface of sample 5.

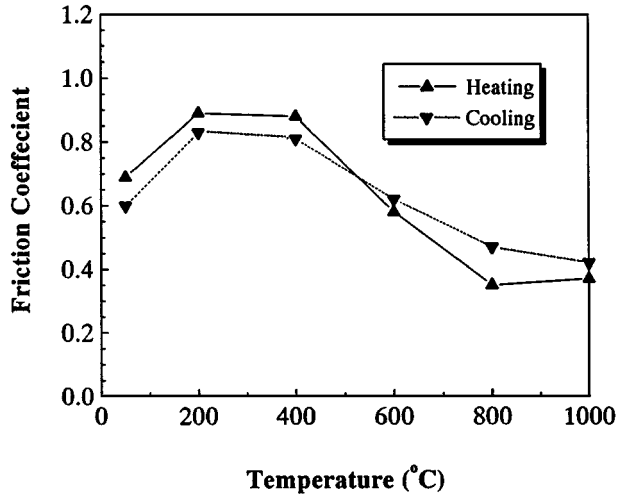

Figure 11 Friction coefficient as a function of temperature.

friction coefficient was in the range of 0.6–0.7, but probably due to the water absorption on the surface this value may not reveal the intrinsic friction coefficient of the sample. After the long duration of sliding and the rising temperature to 200–400 °C the friction coefficient increased to about 0.9. When the temperature was further raised to 600–1000 °C the friction coefficient decreased continuously to about 0.4. Though the friction coefficient in the cooling stage showed the same tendency as in the heating stage, the reason why it decreased at higher temperatures is not clear.

3.4. Oxidation behaviour

The oxidation weight gains of samples held at 1300 °C for 1 h in air are listed in Table IV. The results suggest that the higher content of Ti_3SiC_2 would lead to higher oxidation resistance. Barsoum reported the activation energy of 300 kJ/mol for oxidation [9]. Racault pointed out when the temperature beyond 1050 °C the oxidation reached about 80% and Ti_3SiC_2 was partly protected

TABLE IV Oxidation weight gain of the sintered samples

Processing condition	Ti_3SiC_2 (vol %)	Weight gain (mg/cm^2)
(1600 °C, 40 MPa, 0.5 h)	91	20
(1500 °C, 40 MPa, 0.5 h)	95	14

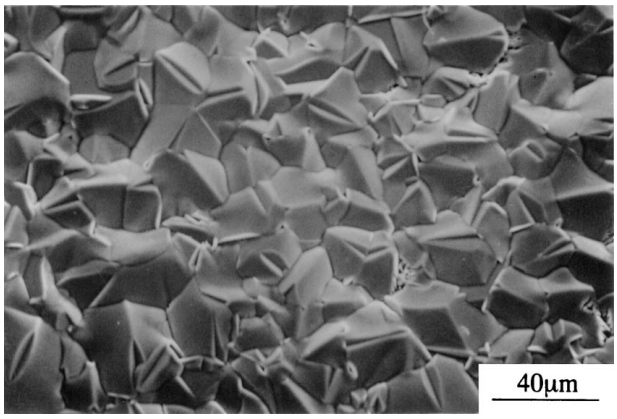

Figure 12 SEM micrograph of the oxidized surface for 1 h at 1300 °C.

against oxidation by cristobalite scale [4]. This oxidation behaviour is not in agreement with the high oxidation resistance reported by Barsoum and El.Raghy.

It is reported by Tong *et al.* that the oxidation resistance could be improved by adding 20 vol % SiC. Both cases showed almost the same weight gain of 14 mg/cm^2 for at 1000 °C for 1 h [15]. The oxidation resistance of reactive HIP samples is higher than the above reported value.

Fig. 12 shows SEM micrograph of the oxidized surface. The surface was covered with TiO_2 grains of 30–50 μm corresponding to the size of Ti_3SiC_2 grains. The occurrence of cracks along the edge of TiO_2 grains seems to be caused by thermal expansion mismatch between Ti_3SiC_2 and TiO_2. According to EDX analysis, there existed no Si on the surface suggesting no formation of SiO_2. Some area of the surface showed the existence of Ti(C,O) indicating partial oxidation of TiC_x.

Considering the above results and TG-DTA analysis as given in Fig. 13, the following reaction of oxidation can be proposed.

(1) In the temperature range of 450–650 °C, $TiC_x + O_2 \rightarrow TiO_2(s) + CO_2(g)$ was the dominant exothermic reaction giving an exothermic peak at 550 °C in DTA curve. In this stage the oxidation of 5 vol % TiC_x impurities gave rise to mild weight increment.

(2) As the temperature went up from 600 to 1100 °C the Ti_3SiC_2 started to decompose following the reaction: $Ti_3SiC_2 \rightarrow TiC_x(s) + Si(s)$, which was probably an endothermic process. The oxidation proceeded resulting in gradual weight gain and the DTA curve went down due to the absorption of heat.

(3) While the temperature above 1100 °C the severe decomposition of Ti_3SiC_2 was highly favored by the oxidation of the TiC_x and vapor phase reaction: $Si(g) + O_2 \rightarrow SiO(g)$, $\Delta G = -450$ kJ/mol.

In a word, no oxidation protection with SiO_2 film and imperfect covering with TiO_2 film allowed the fast oxidation of Ti_3SiC_2 at high temperature. Nevertheless Ti_3SiC_2 was stable up to 1100 °C in oxidation atmosphere.

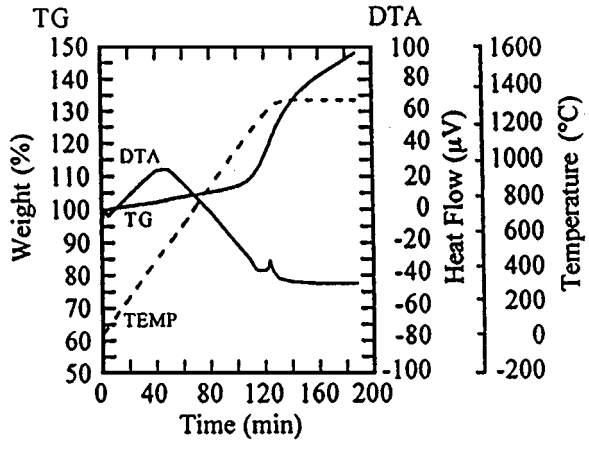

Figure 13 TG-DTA curve of 1 h oxidation at 1300 °C for sample 3.

3.5. Electrical properties

Fig. 14 shows the electrical resistivity of sample 5 as a function of temperature. The Ti_3SiC_2 had the electrical resistivity of 2.7×10^{-7} Ω·m at room temperature, which is smaller than the typical resistivity of graphite. There is a good linear relation between electrical resistivity and temperature showing the metallic behaviour of Ti_3SiC_2. The temperature coefficient was 2.6×10^{-3}/K.

Fig. 15 shows the Seebeck coefficient of Ti_3SiC_2 as a function of temperature. The Seebeck coefficient

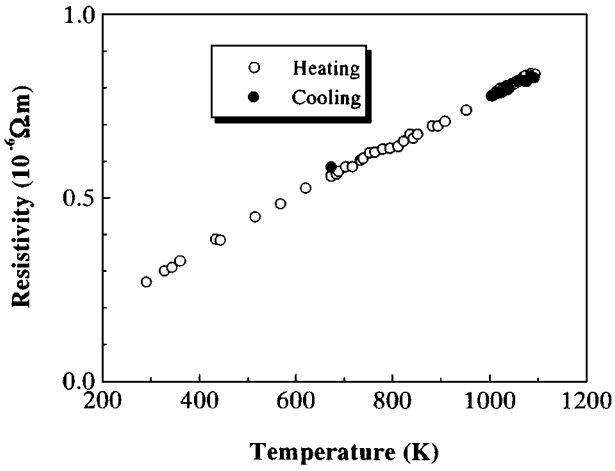

Figure 14 Electrical resistivity as a function of temperature.

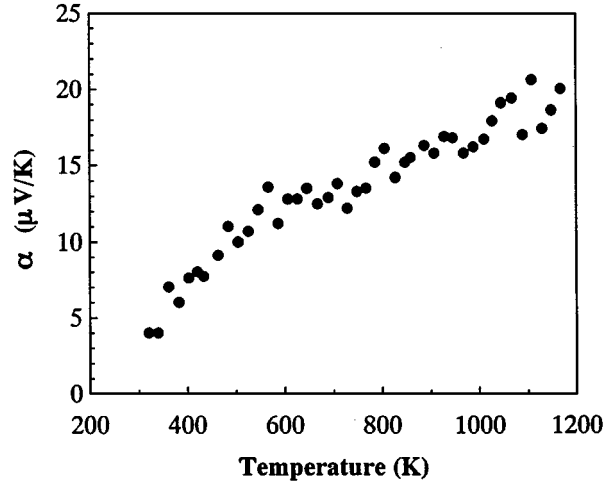

Figure 15 Seebeck coefficient as a function of temperature.

changed in the range from 4 to 20 μV/K between room temperature and 1200 K. This small positive value of Seebeck coefficient and the metallic conductivity suggested that the Ti_3SiC_2 is semi-metal with hole carriers.

4. Conclusions

(1) The dense polycrystalline material consisting of 97 vol % Ti_3SiC_2 and TiC_x as a secondary phase has been synthesized from the mixture of Ti, SiC and C powders by reactive HIP.

(2) The Ti_3SiC_2 grains had columnar and plate-like shapes. Many stacking faults across a grain were observed along the (001) plane.

(3) Ti_3SiC_2 showed a flexural strength of 410 MPa and high fracture toughness of 11.2 MPa $m^{1/2}$. The Vickers hardness of the Ti_3SiC_2 was 12.7 GPa against the indentation load of 49 mN, which decreased with increasing the indentation load and saturated to 4 GPa at over 9.8 N. The higher hardness is attributed to the elastic recovery of Ti_3SiC_2. The Young's modulus is about 283 GPa.

(4) Ti_3SiC_2 was stable up to 1100 °C in air.

(5) The electrical resistivity was 2.7×10^{-7} Ω·m at room temperature. It increased linearly with increasing temperature to 1100 K. The Seebeck coefficient was from 4 to 20 μ V/K in the temperature range of 300–1200 K. The Ti_3SiC_2 is considered as a semimetal with hole carriers.

Further investigation is necessary to clarify the synthesis mechanism of polycrystalline Ti_3SiC_2 and optimize the processing condition to obtain the pure monolithic Ti_3SiC_2.

Acknowledgements

The authors wish to thank Dr. M. V. Swain of CSIRO Division of Applied Physics, Australia, for the help in ultra-micro indentation test, Dr. H. Kido of Osaka Municipal Technical Research Institute, in the measurement of electrical properties, and Dr. K. Umeda of Mechanical Engineering Laboratory, Tsukuba, for the measurement of friction coefficient.

References

1. W. JEITSCHKO and H. NOWOTNY, *Monatash Chem.* **98** (1967) 329.
2. T. GOTO and T. HIRAI, *Mat. Res. Bull.* **22** (1987) 1195.
3. S. MOROZUMI, M. ENDO, M. KIKUCHI and K. HAMAJIMA, *J. Mater. Sci.* **20** (1985) 3976.
4. C. RACAULT, F. LANGLAIS and R. NASLAIN, *ibid.* **29** (1994) 3384.
5. S. ARUNAJATESAN and A. H. CARIM, *J. Amer. Ceram. Soc.* **78** (1995) 667.
6. T. OKANO, T. YANO and T. ISEKI, *Trans. Mat. Res. Soc. Jpn.* **14A** (1993) 597.
7. J. LIS, Y. MIYAMOTO, R. PAMPUCH and K. TANIHATA, *Mater. Lett.* **22** (1995) 163.
8. J. T. LI and Y. MIYAMOTO, Unpublished work.
9. M. W. BARSOUM and T. EL-RAGHY, *J. Mater. Synth. and Process.* **5** (1997) 197.
10. Y. MIYAMOTO, K. TANIHATA, Z. LIS, Y. S. KANG, K. NISHIDA and K. KAWAI, in Proceedings of 8th CIMTEC Conference on Advances in Scinece and Technology edited by P. Vincentini (Techna, Florence, 1995) Vol. 4, p. 387.
11. J. FIELD and M. SWAIN, *J. Mater. Res.* **10** (1995) 101.
12. K. UMEDA, *J. Mech. Eng. Lab.* **50** (1996) 141 (In Japanese).
13. O. YAMADA, Y. MIYAMOTO and M. KOIZUMI, *J. Amer. Ceram. Soc.* **70** (1987) C206.
14. R. PAMPUCH, J. LIS, J. PIEKARCZK and L. STOBIERSKI, *Ceram. Inter.* **19** (1993) 219.
15. X. TONG, T. OKANO, T. ISEKI and T. YANO, *J. Mater. Sci.* **30** (1995) 3087.

Received 25 November 1998
and accepted 15 March 1999